Microporous and Mesoporous Materials 132 (2010) 328–334

Contents lists available at ScienceDirect

Microporous and Mesoporous Materials

journal homepage: www.elsevier.com/locate/micromeso

Two new layered bimetallic sulfides: Solvothermal synthesis, crystal structure, optical and magnetic properties

Zhien Lin [a,*], Xianhui Bu [b], Pingyun Feng [c]

[a] College of Chemistry, Sichuan University, Chengdu 610064, PR China
[b] Department of Chemistry and Biochemistry, California State University, 1250 Bellflower Boulevard, Long Beach, CA 90840, USA
[c] Department of Chemistry, University of California, Riverside, CA 92521, USA

ARTICLE INFO

Article history:
Received 11 February 2010
Received in revised form 12 March 2010
Accepted 13 March 2010
Available online 25 March 2010

Keywords:
Solvothermal synthesis
Layered structure
Bimetallic sulfide
Optical property
Magnetic property

ABSTRACT

Two new bimetallic sulfides, $(Haep)_2{\cdot}Ga_2Sb_2S_7$ (**1**) and $Mn_2(phen)Sb_2S_5$ (**2**), have been synthesized under solvothermal conditions, where aep = 1-(2-aminoethyl)piperazine and phen = 1,10-phenanthroline. The structure of **1** consists of GaS_4 tetrahedra and SbS_3 trigonal pyramids and has a layered structure with 8-membered-ring windows. Interestingly, the interlayer organic cations form helices through extensive hydrogen bonds. Compound **2** has a neutral layered structure containing infinite Mn–S sheets. The organic species are attached directly to Mn atoms within the layers by covalent bonds and protrude into the interlayer region. Both compounds **1** and **2** exhibit intense photoluminescence upon photoexcitation at 360 nm. Magnetic susceptibility measurements demonstrate the existence of antiferromagnetic interactions in compound **2**. Crystal data: **1**, orthorhombic, $P2_12_12_1$ (No. 19), a = 9.9274(2) Å, b = 12.9201(3) Å, c = 21.2254(4) Å, V = 2722.43(10) Å^3, Z = 4; **2**, monoclinic, $P2_1/c$ (No. 14), a = 12.6385(3) Å, b = 12.3998 (3) Å, c = 12.3670(3) Å, β = 111.8240(10)°, V = 1799.19(7) Å^3, Z = 4.

1. Introduction

Crystalline microporous materials have found widespread applications in catalysis, ion exchange, and separation [1–3]. During the past decades, great efforts have focused on the synthesis of new porous materials with new chemical compositions and novel framework topologies because the utilities of these materials are closely related to their compositional and structural features [4–6]. Zeolites (aluminosilicates) are the most well known family of such materials. They are constructed from TO_4 tetrahedra to form three-dimensional structures with open channels or cages. By replacing the framework oxygen atoms with chalcogen atoms, such as S, Se and Te, a large number of open-framework chalcogenides of gallium, indium, germanium, tin, and antimony have been successfully prepared and characterized [7–26]. Unlike those oxide-based microporous materials, which are usually insulators, open-framework metal chalcogenides integrate the semiconductor properties and zeolitic properties into the same crystalline material, which could lead to new applications as photocatalysts, fast ion conductors, photovoltaic materials, etc. [27,28].

Metal chalcogenides with layered structures are of current interest with respect to their potential applications as intercalation hosts and exceptionally selective agents for radioactive elements removal. For example, R–SnS–1 is a well-known nanoporous tin sulfide that possesses a highly flexible layered framework to intercalate a large variety of tetraalkylammonium and amine molecules [29]. The variation of the guest species changes the optical and electrical properties of the host lattice, which indicates the potential application of this material as molecule recognition sensor. Another notable example is $K_{2x}Mn_xSn_{3-x}S_6$ (x = 0.4–0.95), which features hexagonal bimetallic sulfide slabs with highly mobile K^+ ions in their interlayer space that are easily exchangeable with other cations and particularly strontium [30]. To promote specific applications or to enhance particular physical properties, new types of layered metal chalcogenides are often desired. In the present work, we describe the synthesis, structure and characterization of two new layered bimetallic sulfides, $(Haep)_2{\cdot}Ga_2Sb_2S_7$ (**1**) and $Mn_2(phen)Sb_2S_5$ (**2**), where aep = 1-(2-aminoethyl)piperazine and phen = 1,10-phenanthroline. Compound **1** possesses anionic (3,4)-connected inorganic layers intercalated with organic cations. Compound **2** features two-dimensional Mn–S–Mn connectivities in its inorganic–organic hybrid framework.

2. Experimental

2.1. Materials and characterizations

Reagents were purchased commercially and used without further purification. The CHN analyses were carried out on an

* Corresponding author. Fax: +86 28 85418451.
E-mail address: zhienlin@scu.edu.cn (Z. Lin).

1387-1811/$ - see front matter © 2010 Elsevier Inc. All rights reserved.
doi:10.1016/j.micromeso.2010.03.010

Elementar Vario EL III analyzer. Powder X-ray diffraction experiments were performed on a Bruker D8 Advance X-ray powder diffractometer operating at 40 kV and 40 mA (Cu Kα radiation, λ = 1.5418 Å). The data collection was carried out with a step size of 0.02° (2θ) and a counting time of 1 s per step. The thermogravimetric analyses were performed on a Mettler Toledo TGA/SDTA 851e analyzer in a flow of N_2 with a heating rate of 10 K/min from 313 to 1073 K. Diffuse reflectance spectra were recorded at room temperature on a Shimadzu UV-3101PC double-beam, double-monochromator spectrophotometer in the wavelength range of 200–800 nm. $BaSO_4$ powder was used as 100% reflectance reference. The reflectance data were converted to absorbance using the Kubelka–Munk function: $\alpha/S = (1\text{-}R)^2/2R$, where α is the absorption coefficient, S is the scattering coefficient, and R is the reflectance. The photoluminescent spectra were measured on a SPEX Fluorolg-3 Tau3 system equipped with a 450 W xenon lamp and double monochromators on both excitation and emission sides. Magnetic measurements were performed at 5 kG in the temperature range 3–300 K with a SQUID MPMS-7 magnetometer manufactured by Quantum Design. Background corrections for the sample holder assembly and diamagnetic components of the compound were applied.

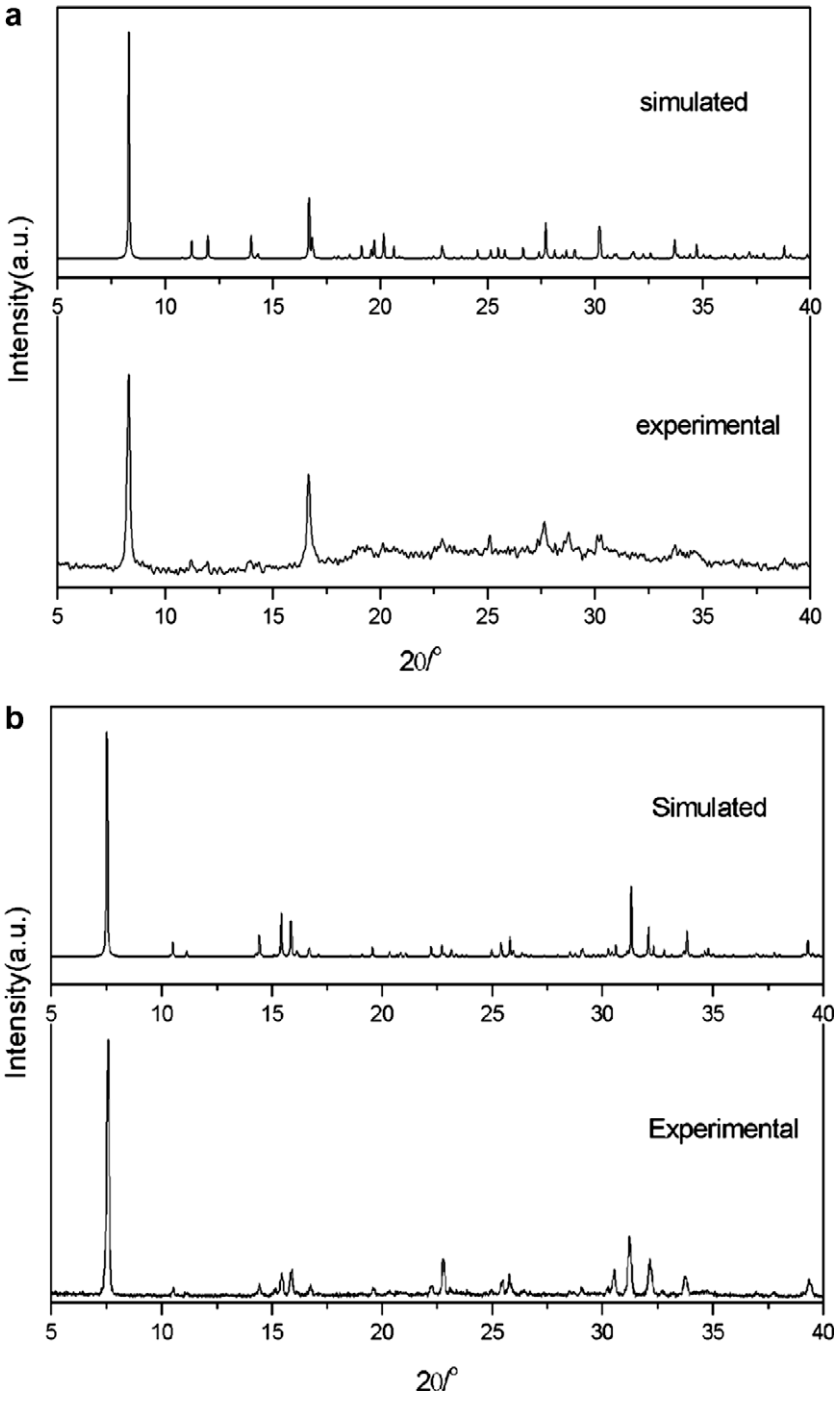

Fig. 1. Experimental and simulated powder X-ray diffraction patterns of (a) compound **1** and (b) compound **2**.

2.2. Synthesis

Compound **1** was synthesized by solvothermal method under autogenous pressure. In a typical synthesis, 0.0632 g of Ga (Aldrich, 99.99%), 0.1104 g of Sb (Aldrich, 99.5%), 0.1740 g of S (Alfa Aesar, 99.5%), and 2.0 g of 1-(2-aminoethyl)piperazine (Alfa Aesar, 98%) in a molar ratio of 1.0:0.9:6.0:16.9 were homogenized for 30 min at room temperature. The mixture was sealed in a 23 ml Teflon-lined stainless steel autoclave and heated at 443 K for 7 d. The autoclave was subsequently allowed to cool to room temperature. The resulting product, consisting of light-yellow plate-like crystals, was recovered by filtration, washed with distilled water, and finally dried at ambient temperature (73% yield based on gallium). CHN analysis confirmed its stoichiometry (Anal. Found: C, 15.88; H, 3.51; N, 9.57%. Calc: C, 16.61; H, 3.72; N, 9.68%). The powder XRD pattern of the resulting product was compared with the one simulated on the basis of the single-crystal structure (Fig. 1a). The diffraction peaks on both patterns corresponded well in position, indicating the purity of the phase.

To prepare compound **2**, 0.339 g of Sb_2S_3 (Aldrich, 99.995%), 0.245 g of $Mn(CH_3COO)_2{\cdot}4H_2O$ (Aldrich, 98%), 0.080 g of S (Alfa Aesar, 99.5%), 0.181 g of phen (Aldrich, 99%), 3.012 g of ethanolamine (Aldrich, 98%) and 1.007 g of H_2O in a molar ratio of 1.0:1.0:2.5:1.0:49.3:55.9 was stirred under ambient conditions for 30 min. The resulting mixture was sealed in a Teflon-lined steel autoclave and heated at 443 K for 7 days and then cooled to room temperature. The dark red single crystals were separated from the resulting product by sonication, washed with distilled water and dried in air (73.5% yield based on manganese). Elemental analyses confirmed its stoichiometry (Anal. Found: C, 19.86; H, 1.05; N, 3.92%. Calc: C, 20.77; H, 1.16; N, 4.04%). The powder XRD pattern of the resulting product was compared with the one simulated on the basis of the single-crystal structure (Fig. 1b). The diffraction peaks on both patterns corresponded well in position, indicating the purity of the phase.

2.3. Crystal structure determination

Crystal structure determination by X-ray diffraction was performed on Bruker APEX II diffractometer with graphite-monochromated Mo Kα ($\lambda = 0.71073$ Å) radiation at 273 K. The empirical absorption correction was based on equivalent reflections, and other possible effects such as absorption by the glass fiber were simultaneously corrected. The crystal structures were solved by direct methods and refined on F^2 by full-matrix least-squares methods using the *SHELXTL* program package [31]. The gallium atoms in compound **1** are disordered over two positions with according site occupancy factors of 0.95:0.05. All the hydrogen atoms were located by calculation and refined using a riding model. All non-hydrogen atoms were refined anisotropically. The crystallographic data for **1** and **2** are summarized in Table 1.

Table 1
Crystal data and structure refinement for **1** and **2.**

	1	2
Empirical formula	$C_{12}H_{32}Ga_2N_6S_7Sb_2$	$C_{12}H_8Mn_2N_2S_5Sb_2$
Formula weight	867.80	693.88
Temperature (K)	293(2)	293(2)
Wavelength (Å)	0.71073	0.71073
Crystal system	Orthorhombic	Monoclinic
Space group	$P2_12_12_1$	$P2_1/c$
a (Å)	9.9274(2)	12.6385(3)
b (Å)	12.9201(3)	12.3998(3)
c (Å)	21.2254(4)	12.3670(3)
β (°)	90	111.824(1)
Volume (Å^3)	2722.43(10)	1799.19(7)
Z	4	4
$\rho_{calc.}$ (g cm^{-3})	2.117	2.562
μ (mm^{-1})	4.472	4.918
Total data	16539	16184
Unique data	4806 [$R_{(int)} = 0.0349$]	3173 [$R_{(int)} = 0.0360$]
Data, $I > 2\sigma(I)$	4410	2385
GOF on F^2	1.038	0.978
Final R indices [$I > 2\sigma(I)$]	$R_1 = 0.0245$, $wR_2 = 0.0534$	$R_1 = 0.0257$, $wR_2 = 0.0514$
R indices (all data)	$R_1 = 0.0280$, $wR_2 = 0.0546$	$R_1 = 0.0426$, $wR_2 = 0.0572$

3. Results and discussion

3.1. Structural description

The structure analysis reveals that compound **1** crystallizes in an enantiomorphous space group $P2_12_12_1$. Its structure consists of anionic inorganic layers with the composition of $[Ga_2Sb_2S_7]^{2-}$. The charge neutrality is achieved by two monoprotonated aep cations per formula unit. The asymmetric unit contains two crystallographically independent Ga atoms and two crystallographically independent Sb atoms, as shown in Fig. 2a. Each Ga atom is tetra-

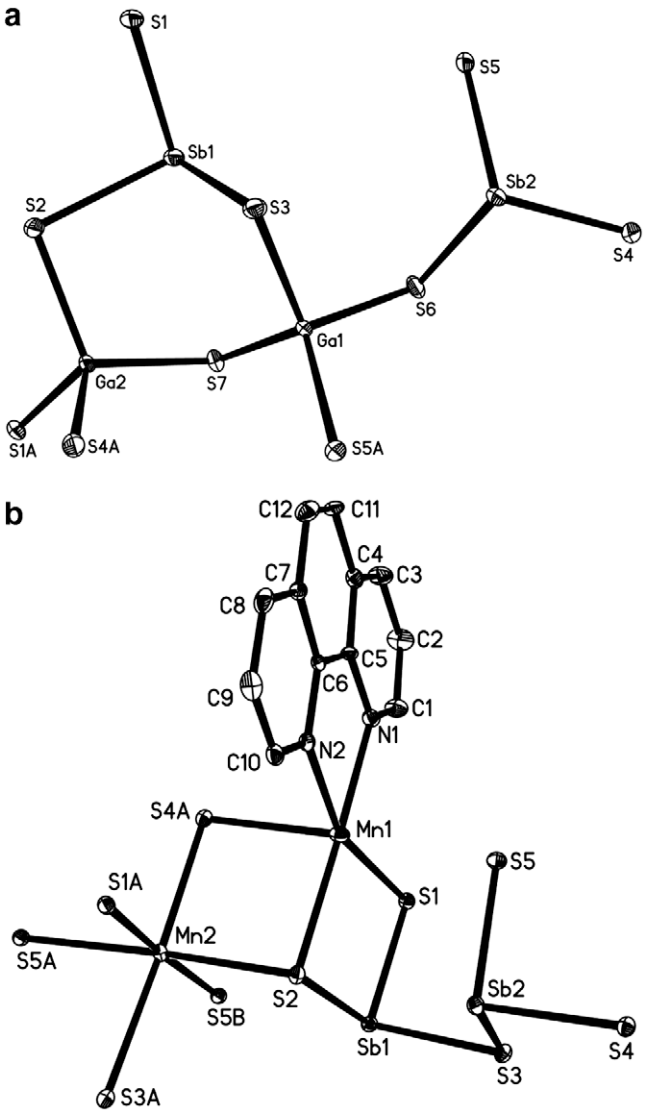

Fig. 2. View of the coordination environment of Ga and Sb atoms in compound **1** (a) and Mn and Sb atoms in compound **2** (b), showing the atom labeling scheme, and with 30% thermal ellipsoids. Atom labels having "A" and "B" refer to symmetry-generated atoms.

hedrally coordinated by their sulfur neighbors with the Ga–S bond lengths in the range of 2.2508(17)–2.2989(17) Å and the S–Ga–S angles in the range of 100.79(7)–113.74(7)°. Each Sb atom is coordinated by three sulfur atoms to form a trigonal pyramidal geometry. The Sb–S bond lengths vary from 2.4039(17) to 2.4630(17) Å, and the S–Sb–S angles are between 90.53(5) and 100.51(6)°, in agreement with those related materials.

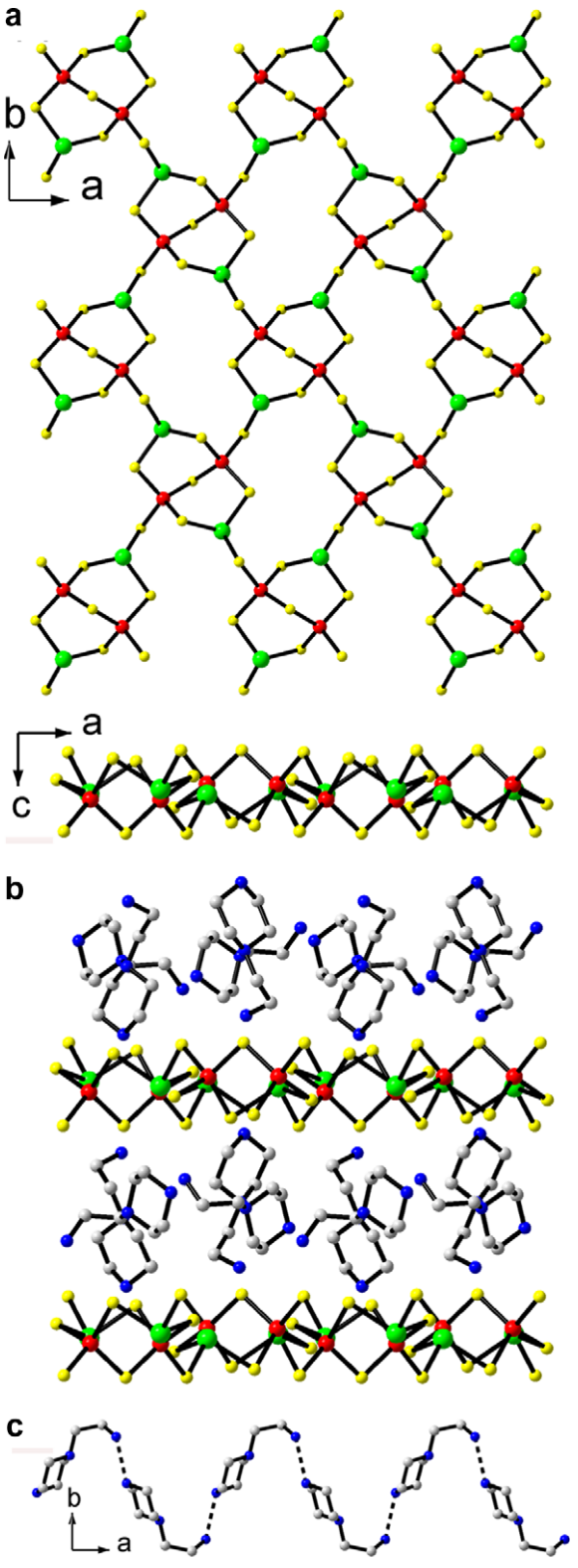

Fig. 3. (a) The sheet-like structure of compound **1** viewed along the [0 0 1] direction. (b) View of the packing of layers along the [0 1 0] direction. (c) A chiral chain formed by the hydrogen-bonded interaction between the organic molecules. The N···N hydrogen bonds are indicated by dotted lines. Color code: Ga, red; Sb, green; S, yellow; N, blue; C, gray. (For interpretation of the references to color in this figure legend, the reader is referred to the web version of this article.)

The layered framework of compound **1** is built from GaS_4 tedrahedra and SbS_3 trigonal pyramids linked through their vertices. The connectivity of these units creates 3- and 8-membered-ring windows, as shown in Fig. 3a. The 3-ring window consists of two GaS_4 tetrahedra and one SbS_3 trigonal pyramid. The 8-ring window, formed by alternating GaS_4 and SbS_3 groups, has the dimensions of 4.3 × 8.8 Å. The presence of Ga–S–Ga linkages in this layered structure is noteworthy. In (3,4)-connected nets, if all 4-connected vertices (denoted A) attach to 3-connected vertices (denoted B) and vice versa, the stoichiometry of the framework will be A_3B_4 [32]. In the case of compound **1**, every SbS_3 unit share its corners with three GaS_4 tetrahedra, and every GaS_4 tetrahedron share its corners with three SbS_3 trigonal pyramids and one GaS_4 tetrahedron. Such connectivity generates a layered structure with a framework composition of $[Ga_2Sb_2S_7]^{2-}$.

The adjacent layers are stacked in an ABAB sequence along the [0 0 1] direction, as shown in Fig. 3b. The interlayer has the thickness of 7.6 Å, calculated as the shortest sulfur-to-sulfur distance between adjacent layers. There are two crystallographically unique monoprotonated amine molecules located in the interlay region. These templating agents are well ordered, perhaps due to the extensive hydrogen bonding between the amino groups and the framework sulfur atoms. The N···S distances are in the range of 3.435(6)–3.797(8) Å.

Interestingly, the organic molecules packed between the inorganic layers also interact with their symmetry-related species through strong hydrogen bonds (N–H···N). The N(4)···N(6) distance is quite short with the value of 2.718(11) Å. As shown in Fig. 3c, these organic molecules are arranged along the 2_1 screw axis and forms a helical chain running along the [1 0 0] direction. Such hydrogen-bonded organic helical chain is particularly rare in chalcogenide materials. It is reminiscent of the hydrogen-bonded helices in a layered aluminophosphate $(C_2H_8N_2)_2[Al_2(HPO_4)(PO_4)_2]$, in which the organic cations interact with the framework oxygen atoms in such a way that hydrogen-bonded helices are created that follow the 2_1 screw axis [33].

An intriguing structural feature of compound **1** is its resemblance to that of $Ga_4Se_7(en)_2{\cdot}(enH)_2$ (en = ethylenediamine) [34]. Both structures contain the same framework topology with 3- and 8-member rings, except that $GaSe_3N$ tetrahedra are replaced by SbS_3 trigonal pyramids. This replacement is remarkable from a structural point of view, since Ga and Sb atoms are greatly different in size and coordination environment. Another difference between the two structures is the role of the organic templates. In the case of $Ga_4Se_7(en)_2{\cdot}(enH)_2$, the organic molecules serve as ligands and structure-directing agents to generate the centrosymmetric structure (space group: $P2_1/c$), whereas in compound **1**, the organic molecules are assembled into helical chains to direct the formation of a chiral solid (space group: $P2_12_12_1$).

The structure analysis reveals that the asymmetric unit of **2** consists of 23 crystallographically independent non-hydrogen atoms, including 2 antimony atoms, 2 manganese atoms, 5 sulfur atoms, 12 carbon atoms and 2 nitrogen atoms (Fig. 2b). Both of the two antimony atoms are coordinated by three sulfur atoms with the Sb–S bond lengths varying from 2.4073(10) to 2.5352(10) Å. Of the two unique manganese atoms, Mn(1) atom bonds to three sulfur atoms and two nitrogen atoms from a phen ligand, forming a distorted square-pyramidal coordination geometry. The Mn–S bond lengths are in the range of 2.550(1)–2.627(1) Å and the Mn–N bond lengths are between 2.251(3) and 2.254(3) Å. Mn(2) atom is octahedrally coordinated by six sulfur atoms with Mn–S bond lengths between 2.540(1) and 2.708(1) Å.

The connectivity between SbS_3 trigonal pyramids, MnS_6 octahedra and MnS_3N_2 square-pyramids create a layered structure, which is parallel to the *bc* plane (Fig. 4a). Interestingly, the layered structure features a two-dimensional Mn–S–Mn connectivity. In such Mn–S sheet, each $M(2)S_6$ octahedron shares one edge with one adjacent $M(2)S_6$ octahedron, one edge with one adjacent $M(2)S_3N_2$ square-pyramid, and one corner with one adjacent $M(2)S_3N_2$ square-pyramid, resulting a layered network with 10-membered ring windows (Fig. 4b).

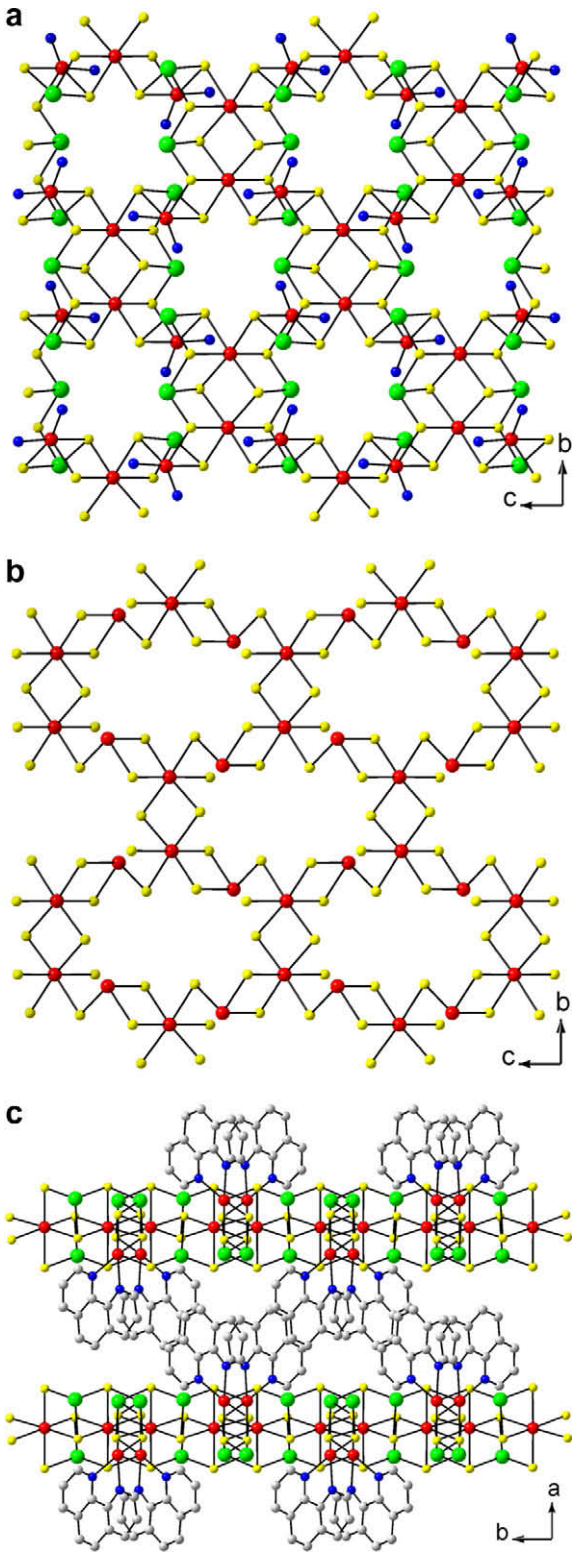

Fig. 4. (a) The layered structure of compound **2** viewed along the [1 0 0] direction. The carbon and hydrogen atoms are omitted for clarity. (b) View of the manganese sulfide layer along the [100] direction. (c) Packing structure of **2** along the [0 0 1] direction. Color code: Mn, red; Sb, green; S, yellow; N, blue; C, gray. (For interpretation of the references to color in this figure legend, the reader is referred to the web version of this article.)

The adjacent layers are stacked in an AAAA sequence along the [1 0 0] direction, as shown in Fig. 4c. Phen ligands are attached directly to Mn atoms within the layers by covalent bonds and protrude into the interlayer region. These organonitrogen ligands between adjacent layers are parallel with each other. The average distance of the adjacent aromatic rings is about 3.34 Å, indicating possible π···π interactions.

It should be noted that a series of manganese antimony sulfides with the general formula of $Mn_2LSb_2S_5$ (L = 1,3-diaminopentane, methylamine, ethylamine, propylamine, diaminopropane, *N*-methylaminopropane and ethylenediamine) has been synthesized and characterized [35–39]. These compounds possess similar bimetallic sulfide layers decorated with organic components. The inorganic–organic hybrid layers interact with each other through van der Waals contacts. However, in the case of compound **1**, π···π interactions between the adjacent layers are also observed.

3.2. Thermal stability

TGA experiment on compound **1** shows that there is no weight change until 543 K, suggesting that the structure remains stable in this period (see Supporting Information Fig. S1). On further heating, a sharp weight loss of 27.66% occurs between 543–673 K, followed by a gradual weight loss of 9.89% between 673 and 873 K. The total weight loss of 37.55% between 543 and 873 K is much higher than the expected value for the decomposition of organic cations (calc. 29.78%). The higher weight loss could be attributes to the partial loss of framework sulfur atoms. Such a phenomenon was also observed in the previous reported open-framework metal sulfide [40]. In the case of compound **2**, two stags of weight loss are observed over the temperature range 313–1073 K (see Supporting Information Fig. S2). The initial weight loss between 573 and 703 K corresponds to the decomposition of the organic molecules (observed: 22.46%; calculated: 25.86%). The remaining organic species was removed from the sample together with framework sulfur atoms at the second stage between 723 and 1073 K with a weight loss of 43.79%.

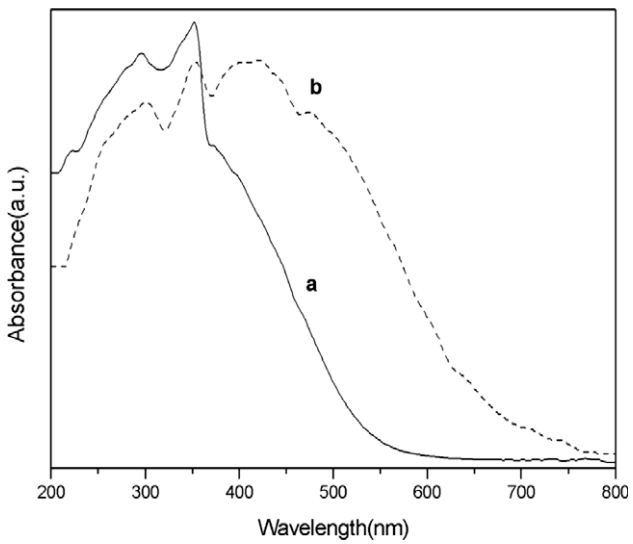

Fig. 5. The diffuse reflection spectra of (a) compound **1** and (b) compound **2**.

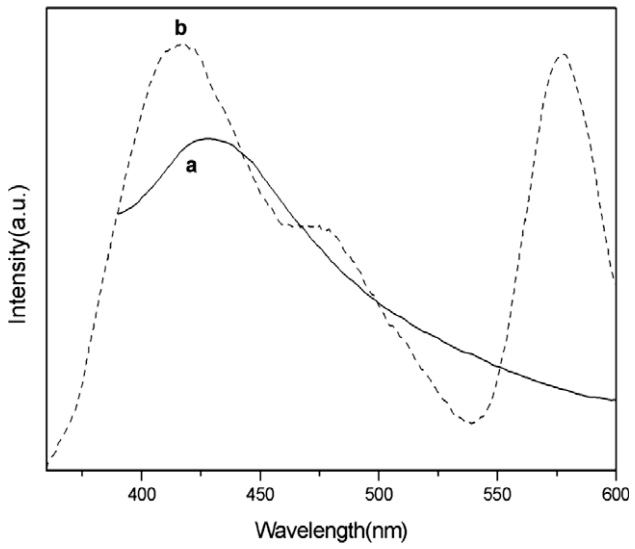

Fig. 6. Room-temperature photoluminescent spectra of (a) compound **1** and (b) compound **2**. The excitation wavelength for the photoluminescent spectra was 360 nm.

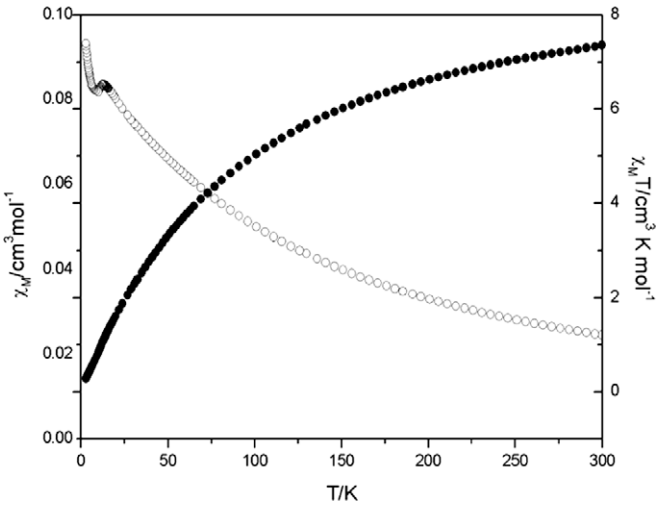

Fig. 7. Temperature dependence of χ_m (○) and $\chi_m T$ (●) curves for compound **2**.

3.3. Diffuse reflectance and photoluminescent spectra

The optical properties of compounds **1** and **2** were studied by solid-state diffuse reflectance spectroscopy. As shown in Fig. 5a, the optical absorption data derived from the reflectance shows an optical transition with a band gap of 2.4 eV. The transition likely results from the S^{2-}-dominated valence band to the Ga^{3+}/Sb^{3+}-dominated conduction band. When excited at 360 nm at room temperature, compound **1** gives an emission band with the maximum wavelength centered at 428 nm (Fig. 6a). In the case of compound **2**, the optical absorption data derived from the reflectance shows an optical transition with a band gap of 1.9 eV (Fig. 5b). The transition likely results from the S^{2-}-dominated valence band to the Mn^{2+}/Sb^{3+}-dominated conduction band. When excited at 360 nm at room temperature, the compound gives two strong emission bands with the maximum wavelength centered at 417 and 578 nm (Fig. 6b), which may be tentatively assigned to intraligand fluorescent emission (for λ_{max} = 417 nm) and ligand-to-metal charge transfer (for λ_{max} = 578 nm).

3.4. Magnetic properties

The temperature dependence of the magnetic susceptibility of **2** was measured at 5000 G in the temperature range 3–300 K. The plot of the molar magnetic susceptibility (χ_m) versus temperature (T) was shown in Fig. 7. The thermal evolution of χ_m follows the Curie–Weiss law at temperature above 50 K, with C_m = 0.10 $cm^3\ K\ mol^{-1}$ and $\theta = -100.57$ K. The value for $\chi_m T$ decreases from 7.36 $cm^3\ K\ mol^{-1}$ at 300 K–0.28 K $cm^3\ K\ mol^{-1}$ at 3 K, indicating the existence of antiferromagnetic interactions. The magnetic moment at 300 K (μ_{eff}) per mole of cobalt atom, determined from the equation $\mu_{eff} = 2.828(\chi_m T/2)^{1/2}$, is 5.43 μ_B, in agreement with the expected spin-only value of Mn(II) in the high spin state (5.92 μ_B). The deviation in μ_{eff} may be caused by spin–orbit coupling of Mn^{II} in the distorted five- and six coordinated environments.

4. Conclusions

Two new layered bimetallic sulfides, $(Haep)_2{\cdot}Ga_2Sb_2S_7$ (**1**) and $Mn_2(phen)Sb_2S_5$ (**2**), were obtained as good quality single crystals under solvothermal conditions. Compound **1** has (3,4)-connected sulfide layers intercalated with organic cations within the interlayer region. Compound **2** has a neutral inorganic–organic hybrid framework with the organic ligands directly attaching to the inorganic scaffold. The two compounds are semiconductors with photoluminescent properties. Magnetic measurements indicate the presence of antiferromagnetic interactions in the structure of **2**.

Acknowledgements

We thank the support of this work by the NNSF of China (Z. L., Grant No. 20801037) and the NSF-CHEM-0809335 (P.F).

Appendix A. Supplementary data

Supplementary data associated with this article can be found, in the online version, at doi:10.1016/j.micromeso.2010.03.010.

References

[1] A. Corma, Chem. Rev. 97 (1997) 2373.
[2] A.K. Cheetham, G. Férey, T. Loiseau, Angew. Chem. Int. Ed. 38 (1999) 3268.
[3] M.E. Davis, Nature 417 (2002) 813.
[4] J. Yu, R. Xu, Acc. Chem. Res. 36 (2003) 481.
[5] E.R. Parnham, R.E. Morris, Acc. Chem. Res. 40 (2007) 1005.
[6] S. Natarajan, S. Mandal, Angew. Chem. Int. Ed. 47 (2008) 4798.
[7] R.L. Bedard, L.D. Vail, S.T. Wilson, E.M. Flanigen, US Patent 4880,761, 1989.
[8] J.B. Parise, Science 251 (1991) 293.
[9] O.M. Yaghi, Z. Sun, D.A. Richardson, T.L. Groy, J. Am. Chem. Soc. 116 (1994) 807.
[10] C.L. Cahill, Y. Ko, J.B. Parise, Chem. Mater. 283 (1998) 1145.
[11] T. Jiang, G.A. Ozin, J. Mater. Chem. 8 (1998) 1099.
[12] H. Li, A. Laine, M. O'Keeffe, O.M. Yaghi, Science 283 (1999) 1145.
[13] C. Wang, X. Bu, N. Zheng, P. Feng, Angew. Chem. Int. Ed. 41 (2002) 1959.
[14] W. Su, X. Huang, J. Li, H. Fu, J. Am. Chem. Soc. 124 (2002) 12944.
[15] M.K. Brandmayer, R. Clérac, F. Weigend, S. Dehnen, Chem. Eur. J. 10 (2004) 5147.
[16] P. Vaqueiro, A.M. Chippindale, A.V. Powell, Inorg. Chem. 43 (2004) 7963.
[17] X. Bu, N. Zheng, P. Feng, Chem. Eur. J. 10 (2004) 3356.
[18] P. Feng, X. Bu, N. Zheng, Acc. Chem. Res. 38 (2005) 293.
[19] S. Dehnen, M. Melullis, Coord. Chem. Rev. 251 (2007) 1259.
[20] N. Ding, M.G. Kanatzidis, Chem. Mater. 19 (2007) 3867.
[21] M.J. Manos, C.D. Malliakas, M.G. Kanatzidis, Chem. Eur. J. 13 (2007) 51.
[22] P. Vaqueiro, M.L. Romero, J. Am. Chem. Soc. 130 (2008) 9630.
[23] M.-L. Feng, D.-N. Kong, Z.-L. Xie, X.-Y. Huang, Angew. Chem. Int. Ed. 47 (2008) 8623.
[24] M.-L. Feng, Z.-L. Xie, X.-Y. Huang, Inorg. Chem. 48 (2009) 3904.
[25] J. Zhou, J. Dai, G.-Q. Bian, C.-Y. Li, Coord. Chem. Rev. 253 (2009) 1221.
[26] S. Haddadpour, M. Melullis, H. Staesche, C.R. Mariappan, B. Roling, R. Clérac, S. Dehnen, Inorg. Chem. 48 (2009) 1689.
[27] N. Zheng, X. Bu, H. Vu, P. Feng, Angew. Chem. Int. Ed. 44 (2005) 5299.
[28] N. Zheng, X. Bu, H. Vu, P. Feng, Nature 426 (2003) 428.

[29] H. Ahari, C.L. Bowes, T. Jiang, A. Lough, G.A. Ozin, R.L. Bedard, S. Petrov, D. Young, Adv. Mater. 7 (1995) 375.
[30] M.J. Manos, N. Ding, M.G. Kanatzidis, Proc. Natl. Acad. Sci. USA 105 (2008) 3696.
[31] G.M. Sheldrick, SHELXTL 5.1, Bruker AXS Inc., Madison, WI, USA, 1997.
[32] M. O'Keeffe, M. Eddaoudi, H. Li, T. Reineke, O.M. Yaghi, J. Solid State Chem. 152 (2000) 3.
[33] Y. Song, J. Yu, Y. Li, G. Li, R. Xu, Angew. Chem. Int. Ed. 43 (2004) 2399.
[34] Y. Dong, Q. Peng, R. Wang, Y. Li, Inorg. Chem. 42 (2003) 1794.
[35] A. Puls, C. Näther, W. Bensch, Z. Anorg. Allg. Chem. 632 (2006) 1239.
[36] L. Engelke, R. Stähler, M. Schur, C. Näther, W. Bensch, R. Pöttgen, M.H. Möller, Z. Naturforsch. 59b (2004) 869.
[37] M. Schur, W. Bensch, Z. Naturforsch. 57b (2002) 1.
[38] W. Bensch, M. Schur, Eur. J. Solid State Inorg. Chem. 33 (1996) 1149.
[39] M. Schur, C. Näther, W. Bensch, Z. Naturforsch. 56b (2001) 79.
[40] H. Li, J. Kim, T.L. Groy, M. O'Keeffe, O.M. Yaghi, J. Am. Chem. Soc. 123 (2001) 4867.